Fluorescent Nanoclusters

DOI: 10.1002/ange.201307480

A 200-fold Quantum Yield Boost in the Photoluminescence of Silver-Doped Ag_xAu_{25-x} Nanoclusters: The 13th Silver Atom Matters**

Shuxin Wang, Xiangming Meng, Anindita Das, Tao Li, Yongbo Song, Tiantian Cao, Xiuyi Zhu, Manzhou Zhu, and Rongchao Jin**

Abstract: *The rod-shaped Au_{25} nanocluster possesses a low photoluminescence quantum yield (QY = 0.1 %) and hence is not of practical use in bioimaging and related applications. Herein, we show that substituting silver atoms for gold in the 25-atom matrix can drastically enhance the photoluminescence. The obtained Ag_xAu_{25-x} (x = 1–13) nanoclusters exhibit high quantum yield (QY = 40.1 %), which is in striking contrast with the normally weakly luminescent Ag_xAu_{25-x} species (x = 1–12, QY = 0.21 %). X-ray crystallography further determines the substitution sites of Ag atoms in the Ag_xAu_{25-x} cluster through partial occupancy analysis, which provides further insight into the mechanism of photoluminescence enhancement.*

Fluorescent nanomaterials are of major importance in many fields.[1–4] Different types of fluorescent nanomaterials have been developed, such as quantum dots (QDs),[5] lanthanide nanoparticles,[6,7] and carbon nanodots.[8,9] Metal nanoclusters (Ag, Au) have emerged as a new class of nanomaterial.[10–23] Compared to QDs,[24] Au and Ag nanoclusters (NCs) are more biocompatible and can be readily bioconjugated; other advantages include their extrememly small size, good photostability, and low toxicity; thus, fluorescent noble-metal NCs have been recognized as a promising candidate for cell labeling, biosensing, and photo-therapy applications.[25–30] However, a general issue lies in the lower quantum yield (QY) of metal NCs compared to QDs and organic dyes, which significantly limits the applications of metal NCs. Various approaches have been developed to synthesize noble metal NCs with enhanced fluorescence, for example: 1) engineering the particle surface by using different ligands, such as DHLA,[31] dendrimers,[32] polymers,[33] DNA,[34,35] peptides, and proteins;[36–44] 2) controlling the metal core size[45] or doping the core with other metal atoms. Doping atomically precise nanoclusters is highly desired and allows atomic-level insight into the origin of fluorescence, which is of major importance.[46,47] Recently, several doped gold NCs with conserved core size have been successfully synthesized;[48–53] however, these thiolate-protected nanoclusters, as well as the phosphine-protected gold NCs,[13,16,54] are of low fluorescence.

Herein, we report the discovery of drastic fluorescence enhancement in gold nanoclusters doped with 13 Ag atoms. Interestingly, gold nanoclusters of the same structure, but doped with fewer Ag atoms, are only weakly fluorescent. Thus, the 13th Ag atom triggers strong fluorescence in the doped gold nanocluster.

Two synthetic methods were devised for obtaining Ag-doped, 25-metal-atom nanoclusters (see the Experimental Section and the Supporting Information for details). In the first route, polydisperse Au nanoparticles[16] were first made and then used as the precursors to react with an Ag^I thiolate complex, which gave rise to Ag-doped gold nanoclusters with 25 metal atoms (**I**). In a second synthetic route, Au_{11} nanoclusters[13] (as opposed to the nanoparticles used in the first route) were first prepared and then reacted with Ag^I thiolate to form Ag-doped nanoclusters of 25 metal atoms (**II**). Characterization of phosphine-protected Au_{11} NCs and small Au nanoparticles are provided in the Supporting Information, Figure S1. For comparison, we also prepared undoped Au_{25} nanoclusters.[13,16]

Electrospray ionization time-of-flight mass spectrometry (ESI-TOF MS) was employed to characterize the Au/Ag alloy nanoclusters and the undoped Au_{25} (Figure 1). The undoped Au_{25} NCs[16] are formulated as $[Au_{25}(PPh_3)_{10}(SC_2H_4Ph)_5Cl_2]^{2+}$, and exhibit a clean signal at m/z 4151.8 (Figure 1a), which is consistent with the expected value (4151.6; FW = 8303.2 and charge number (z) = 2). In contrast, the Au/Ag alloy nanoclusters showed a series of peaks corresponding to different numbers of Ag atoms doped into the gold clusters (Figure 1b for **I** and Figure 1c for **II**). This was evidenced by the mass difference between peaks equal to the gold and silver atomic mass difference (197–108 = 89 Da), thus forming a distribution of $[Ag_xAu_{25-x}(PPh_3)_{10}(SC_2H_4Ph)_5Cl_2]^{2+}$, but with the total number of metal atoms preserved at 25. A distinct difference between **I** and **II** lies in the attained maximum number of Ag

[*] S. Wang, X. Meng, Y. Song, T. Cao, X. Zhu, Prof. M. Zhu
Department of Chemistry, Anhui University
Hefei, Anhui 230601 (China)
E-mail: zmz@ahu.edu.cn
A. Das, Prof. R. Jin
Department of Chemistry, Carnegie Mellon University
Pittsburgh, PA 15213 (USA)
E-mail: rongchao@andrew.cmu.edu
T. Li
Department of Chemistry, University of Pittsburgh
Pittsburgh, PA 15213 (USA)

[**] M.Z. acknowledges financial support by NSFC (20871112, 21072001, 21372006), Chang Jiang Scholars Program and the Scientific Research Foundation for Returning Overseas Chinese Scholars, State Education Ministry and Ministry of Human Resources and Social Security, Anhui Province International Scientific and Technological Cooperation Project, 211 Project of Anhui University. R.J. acknowledges support by the Air Force Office of Scientific Research under AFOSR Award No. FA9550-11-1-9999 (FA9550-11-1-0147).

Supporting information, including characterization of nanoclusters, cytotoxicity assays, and fluorescence microscopy imaging experiments, for this article is available on the WWW under http://dx.doi.org/10.1002/anie.201307480.

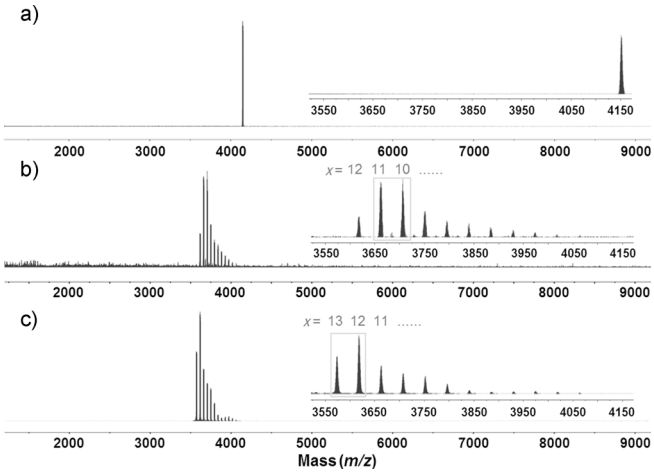

Figure 1. ESI mass spectra of: a) $[Au_{25}(PPh_3)_{10}(SC_2H_4Ph)_5Cl_2]^{2+}$, b) **I**, and c) **II**. The general formula of **I** and **II** is $[Ag_xAu_{25-x}(PPh_3)_{10}(SC_2H_4Ph)_5Cl_2]^{2+}$, but with different x ranges.

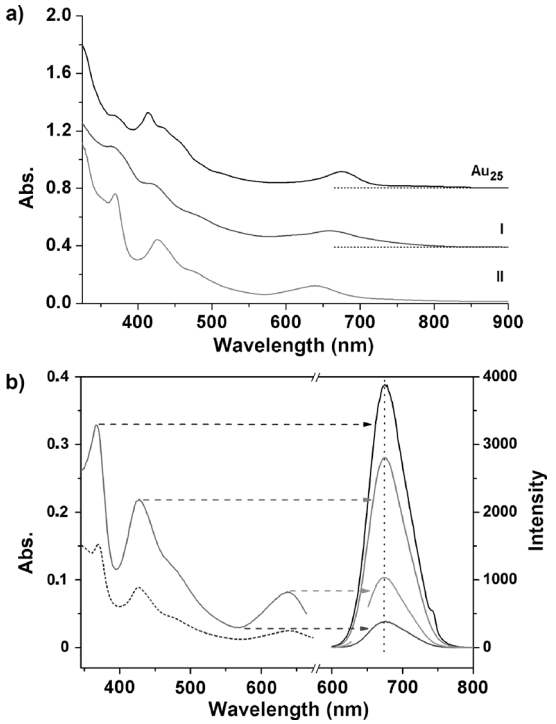

Figure 2. a) UV/Vis spectrum of Au_{25}, **I**, and **II**, the inset is a photo of the cluster solutions. b) photoluminescence properties of product **II**. PLE (——), UV/Vis (-----). UV/Vis and excitation spectra (left), and emission spectra (right) at different excitation wavelengths, as indicated by arrows.

dopants in the cluster. Route 1, with Au nanoparticles as the starting material, gave rise to a maximum doping of 12 Ag atoms (Figure 1b, inset). In route 2, Au_{11} clusters were used as the starting material, and we obtained a unique 13-Ag-atom doped $Ag_{13}Au_{12}$ nanocluster with the same ligands as in the $[Au_{25}(PPh_3)_{10}(SC_2H_4Ph)_5Cl_2]^{2+}$ (and hence omitted hereafter), in addition to the Ag_xAu_{25-x} species ($x \leq 12$) observed in synthetic route 1. The isotope patterns of $Ag_{13}Au_{12}$, $Ag_{12}Au_{13}$, and Au_{25} match closely with the simulated patterns (Figures S2–S4), and so do the isotope patterns of other Ag_xAu_{25-x} species, thus confirming the formula assignment.

The optical properties of $[Au_{25}(PPh_3)_{10}(SC_2H_4Ph)_5Cl_2]^{2+}$ exhibit high sensitivity to the number of Ag atoms doped into the cluster. Figure 2a shows that the Au_{25} clusters have distinct absorption bands centered at 413 nm and 675 nm; the latter is the HOMO–LUMO transition.[55,56] With Ag atoms substituted into the gold cluster, the 675 nm band blue shifts and gives rise to a color change of the cluster solution from brown to green. Drastic spectral changes occur in the spectrum of **II**, in which two pronounced bands at 370 nm and 427 nm were observed in addition to the further blue shift of the HOMO–LUMO peak; these features are thus primarily caused by the substitution of the 13th Ag atom into the cluster, indicating strong perturbation to the electronic structure of the cluster by the 13th Ag atom.

Product **I** exhibits a weak emission at ca. 720 nm (Figure S5) with a quantum yield of only 0.21%, thus indicating that all the Ag_xAu_{25-x} species with $x \leq 12$ are weakly fluorescent. Of note, the undoped Au_{25} clusters also exhibit a weak emission at about 827 nm with a low quantum yield (ca. 0.1%), which is consistent with the report of Park and Lee.[54] Significantly, doped **II** exhibits drastically enhanced photoluminescence with a quantum yield of 40.1%, and the emission band blue shifts to about 680 nm (Figure 2b). A comparison of the photoluminescence (PL) of Au_{25} and **I** and **II** are shown in Figure S5. An interesting question is: which specific species in the Ag_xAu_{25-x} distribution (**II**) is strongly fluorescent? As all of the Ag_xAu_{25-x} species with $x \leq 12$ (**I**) are weakly fluorescent, the 13-Ag-atom doped nanocluster in **II** is responsible for the observed high fluorescence. The PL excitation spectrum of **II** (Figure 2b, left, solid profile) is almost identical with the absorption spectrum (Figure 2b, left, dotted profile); this behavior is reminiscent of quantum-dot behavior.[24] It is noteworthy that the emission peak wavelength is not dependent on the excitation wavelength (Figure 2b).

Compared to **I**, it is surprising that the unique $Ag_{13}Au_{12}$ species in **II** shows a significantly increased quantum yield, which implies that, when Ag dopants reach 13 atoms, a large perturbation to the electronic relaxation and dynamics of the resultant $Ag_{13}Au_{12}$ cluster occurs. To elucidate the structural and electronic origin of the high fluorescence of the doped nanoclusters, we carried out full characterization of the as-obtained products.

The $[Ag_xAu_{25-x}(PPh_3)_{10}(SC_2H_4Ph)_5Cl_2]^{2+}$ nanoclusters obtained in routes 1 and 2 allow the growth of single crystals. X-ray crystallography was used to determine the structure of the doped nanoclusters (Figure 3). First, all three types of nanoclusters (Au_{25}, and Ag-doped **I** and **II**) adopt the same biicosahedral structure.[13,16] As the $[Ag_xAu_{25-x}(PPh_3)_{10}(SC_2H_4Ph)_5Cl_2]^{2+}$ nanoclusters have different numbers of Ag atoms, and X-ray crystallography only gave an average electron-density map, we carried out partial occupancy analysis to pinpoint the specific sites for Ag dopants in the biicosahedral structure. Partial occupancy analysis indicates that in both **I** and **II** the top and bottom vertex positions (Figure 3b,c) are essentially occupied by silver atoms, which is

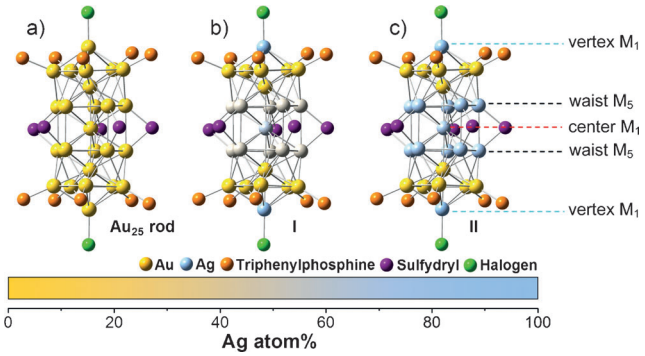

Figure 3. X-ray structures of: a) $[Au_{25}(PPh_3)_{10}(SC_2H_4Ph)_5Cl_2]^{2+}$, b) **I**, and c) **II**. M = metal atom.

in contrast with Au vertices in the homogold Au_{25} nanocluster (Figure 3a); this is due to the fact that these two vertex sites are bound to Cl, and Ag has a higher affinity to halogens than does Au. Product **I** contains a series of Ag_xAu_{25-x} species ($x \leq 12$, with 10 and 11 being the most abundant; see Figure 1b, inset); they possess the same biicosahedral geometric structure (Figure 3b). Partial occupancy analysis also shows that the metal atoms at the "waist" (Figure 3b, grey) are randomly occupied by Au and Ag with roughly equal probability (silver occupancy of ca. 45%, average of all the Ag_xAu_{25-x} clusters in the crystal), and that the biicosahedral center is randomly occupied by Au and Ag with a Ag occupancy of 65%. In **II**, gold atoms at the waist sites (Figure 3c, cyan) were replaced by silver atoms at a much higher probability (ca. 80%), including the center (ca. 76% occupancy of Ag). The much higher Ag occupancy in **II** is consistent with ESI-TOF analysis, in which the Ag_xAu_{25-x} species ($x \leq 13$, with 12 and 13 being the most abundant; see Figure 1c, inset). This difference significantly influences the photoluminescence of **I** and **II**.

^{1}H NMR analysis provides additional evidence for the replacement of gold by silver atoms at the waist of the 25-metal-atom structure. For the thiolate ligand in the cluster, the α-CH_2 (relative to the -SH group) is the closest to the metal core, and thus can probe the metal atom to which the thiolate ligand is bonded.[57] In Figures S6–S8, the ^{1}H NMR signal of the α-CH_2 shifts distinctly from 3.71 to 2.93 ppm with increasing silver doping. The ^{31}P NMR spectrum (Figure S9) also suggests that the substitution occurs on the waist, rather than at the top and bottom pentagons of the rod, because the ^{31}P signals did not shift. ^{1}H-^{1}H COSY further verifies that **II** (Figure S10) and **I** (Figure S11) have the same structure as that of the Au_{25} nanocluster (Figure S12), because the ^{1}H-^{1}H correlations of the ligands are almost the same.

Previously, Lee et al. reported that the HOMO–LUMO gap of Au_{25} nanorods is 1.54 eV (805 nm), which is close to the emission wavelength of the Au_{25} rod cluster (827 nm).[54] We performed differential pulse voltammetry (DPV) and square wave voltammetry (SWV) analyses of **II** (Figure S13). The HOMO–LUMO gap was determined to be 1.79 eV (690 nm), which is also very close to the emission wavelength (680 nm). These results suggest that the fluorescence of both Au_{25} nanorods and **II** originates from the LUMO–HOMO transition; thus, electronic perturbation to the HOMO and LUMO orbitals would largely influence the fluorescence properties. It is intriguing that Au_{25} nanorods are essentially non-fluorescent (QY ≈ 0.1%), whereas their silver-doped counterparts (**II**) emit strong fluorescence. In terms of the electronic structure of the Au_{25} rod cluster,[55,56] the HOMO orbital is localized on the ten gold atoms at the waist, and contributed by Au 6s and 6p atomic orbitals, whereas the LUMO orbital is highly localized on the central Au atom (Figure S14). According to the X-ray structural analysis of Ag-doped rod clusters, Ag atoms first preferentially substitute for the two vertex Au atoms, then the ten Au atoms at the waist and the Au atom in the center (Figure 3). When the 13 Au atoms are replaced, strong perturbation to the electronic structure occurs, manifested in the UV/Vis spectral profile and photoluminescence intensity. Gold atoms show a strong sd hybridization owing to the relativistic effect; the LUMO (which consists of the Au 6s and 6p orbitals) will be largely altered after the 13 Au atoms are substituted by Ag atoms, as the Ag 5s orbital is higher than the Au 6s; this gives rise to a larger energy gap and explains the blue shift of the HOMO–LUMO transition. The fluorescence relates to the recombination rate of the photoexcited electron (on the LUMO) and the hole (on the HOMO). Silver substitution of the 13 Au atoms (i.e. the case of $Ag_{13}Au_{12}$) results in a HOMO and LUMO consisting completely of Ag 5s, rather than mixed Au 6s and Ag 5s (i.e. the cases of weakly fluorescent Ag_xAu_{25-x}, $x < 13$). Compared to Au 6s, the effective mass of Ag 5s electrons is closer to one, owing to less sd hybridization in Ag, and hence, higher electron mobility in the $Ag_{13}Au_{12}$ cluster than in Au_{25}. Furthermore, the closer masses of the excited electron and the hole in $Ag_{13}Au_{12}$ should contribute to a higher recombination rate, thus, giving off stronger photoluminescence in the 13-substituted $Ag_{13}Au_{12}$ nanocluster. Single crystals of **II** also exhibit strong red luminescence, that is, no solid-state quenching of fluorescence occurs.

With respect to the metal–sulfur (M–S) bond length change after Ag doping (Table S1), **I** gives rise to an average increase of 0.09 Å (3.8%) over Au_{25}, and **I** and **II** give comparable M–S bond lengths (2.42 vs. 2.41 Å; Table S1). Therefore, the M–S bond length change is not relevant to the large photoluminescence enhancement. We have also compared the M–M bonds, but no appreciable change was found (Table S1).

The extraordinary PL properties of **II** hold potential for biological applications. However, the phenethyl group in the ligand renders the nanoclusters water insoluble, and functionalization of the nanoclusters by biomolecules is also an issue. To solve these problems, we introduced hydroxyethylthiol in the synthesis of **II**. The as-obtained $[Ag_xAu_{25-x}(PPh_3)_{10}(SC_2H_4OH)_5Cl_2]^{2+}$ ($x \leq 13$) nanoclusters were tested in living cells (human cancer cell 7402). Fluorescence confocal imaging of these NCs-labeled cells (Figure 4) was done by monitoring red PL from the nanoclusters (excitation: 405 nm or 633 nm laser), which displays intracellular staining after incubation at 37 °C for 2 h. The wide excitation wavelength range and the red emission make this nanocluster feasible for simultaneous use with other dyes with emission shorter than 600 nm (e.g. the most MitoTracker and LysoTracker) without

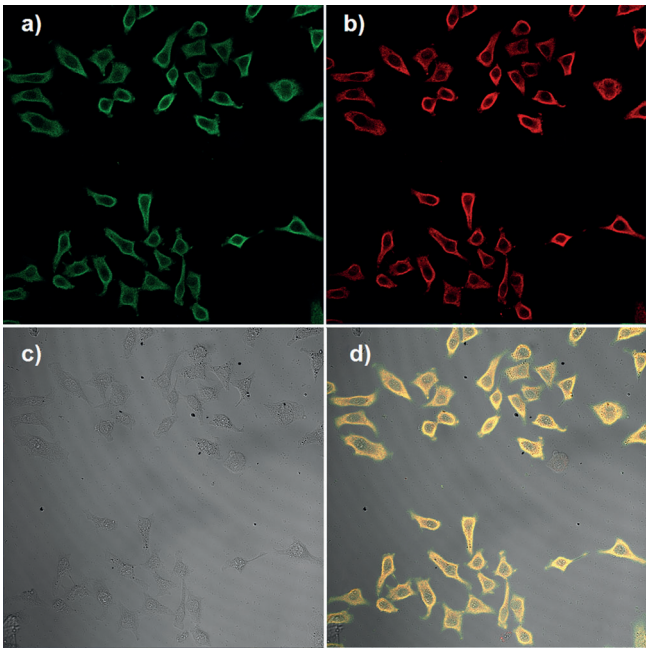

Figure 4. a) Confocal image (false color) of human cancer cells (7402) incubated with 10 μg mL^{-1} $[Ag_xAu_{25-x}(PPh_3)_{10}(SC_2H_4OH)_5Cl_2]^{2+}$ ($x = 2$–13) after 2 h of incubation, washed by PBS buffer. $\lambda_{ex} = 405$ nm (emission wavelength from 650–750 nm). b) $\lambda_{ex} = 633$ nm (emission wavelength from 650–750 nm). c) Bright-field image of 7402 cells. d) Overlay of (a), (b), and (c).

any interference. The 5-dimethylthiazol-2-yl-2,5-diphenyltetrazolium bromide (MTT) assay demonstrates that the nanocluster probe shows no cytotoxicity after a long period of incubation (Figure S16).

In summary, we have identified a highly fluorescent $Ag_{13}Au_{12}$ nanocluster by comparing two series of Ag-doped Ag_xAu_{25-x} nanoclusters prepared by two different routes. The reaction of Au nanoparticles with Ag^I thiolate gives rise to Ag_xAu_{25-x} with $x \leq 12$, with all of these species only weakly fluorescent (QY $\approx 0.2\,\%$). Reaction of Au_{11} clusters with Ag^I thiolate gives rise to Ag_xAu_{25-x} with $x \leq 13$, and the unique $Ag_{13}Au_{12}$ species in the distribution is highly luminescent (QY $\approx 40.1\,\%$). Structural analysis shows that the Ag_xAu_{25-x} nanoclusters are geometrically identical and adopt the same biicosahedral structure. Significantly, only when the 13 Au sites that are associated with the HOMO and LUMO are fully substituted with silver does the alloy cluster become highly fluorescent. The atomic-level structural and electronic insight provides a promising design principle for highly fluorescent metal nanoclusters, and may stimulate future work on the deep understanding of the atomic-level origin of fluorescence from metal nanoclusters, as well as on the development of applications in biolabeling, sensing, and other fields.

Experimental Section

Synthesis of phosphine-protected Au nanoparticles and conversion to $[Ag_xAu_{25-x}(PPh_3)_{10}(SR)_5Cl_2]^{2+}$ ($x \leq 12$; **I**): Triphenylphosphine-capped Au nanoparticles were prepared by $NaBH_4$ reduction of $HAuCl_4$ in a water/toluene system in the presence of tetraoctylammonium bromide (TOAB) and PPh_3.[16] The obtained polydisperse nanoparticles were then used as the precursor for the synthesis of alloy nanocluster **I** by reaction with phenethylthiosilver. PhC_2H_4SAg (80 mg) was added to the ethanol solution (10 mL) of nanoparticles (75 mg) under vigorous stirring at 298 K. After 6 h, the product was dried in vacuum, washed several times with ethanol/hexane (1:3, V/V), redissolved in a minimal amount of methanol, and purified by a Sephadex LH-20 column. The brownish-yellow fraction that eluted first was collected and mixed with an excess of $NaSbF_6$ for 15 min. Insoluble products were collected on a filter and crystallized from a mixed solution of CH_2Cl_2 and diethyl ether.

Synthesis of $[Au_{11}(PPh_3)_8Cl_2]^+$and conversion to $[Ag_xAu_{25-x}(PPh_3)_{10}(SR)_5Cl_2]^{2+}$ ($x \leq 13$; **II**): Triphenylphosphine-stabilized Au_{11} clusters were prepared by the method described in Ref. S3. Then, Au_{11} was reacted with alkanethiosilvers (including (2-hydroxyethylthio)-silver and phenethylthiosilver). In the case of phenethylthiosilver, PhC_2H_4SAg (80 mg, 0.33 mmol) was added to an ethanol solution (10 mL) of Au_{11} NCs (75 mg, 0.017 mmol) under vigorous stirring at 313 K. After 6 h, the product was dried under vacuum, washed several times with ethanol/hexane (1:3, V/V), redissolved in a minimal amount of methanol, and passed through a Sephadex LH-20 column. The dark green fraction that was eluted first was collected, then mixed with excess $NaSbF_6$ for 15 min. Insoluble products were collected after centrifugation, crystallized from a mixed solution of CH_2Cl_2 and diethyl ether. The synthetic procedure that uses functionalized groups (2-hydroxyethylthio)silver is slightly different in reaction temperature. $CH_2(OH)CH_2SAg$ (56 mg, 0.33 mmol) was added to the ethanol solution (10 mL) of Au_{11} NCs (75 mg, 0.017 mmol) under vigorous stirring at 293 K. The products were dried in vacuo, washed several times with ethanol/hexane (1:3, V/V), redissolved in a minimal amount of methanol, and finally purified by a Sephadex LH-20 column.

Received: August 26, 2013
Revised: November 11, 2013
Published online: January 28, 2014

Keywords: doping · gold · metal nanoclusters · photoluminescence · silver

[1] J. Liu, M. Yu, C. Zhou, S. Yang, X. Ning, J. Zheng, *J. Am. Chem. Soc.* **2013**, *135*, 4978.
[2] C. I. Richards, J.-C. Hsiang, D. Senapati, S. Patel, J. Yu, T. Vosch, R. M. Dickson, *J. Am. Chem. Soc.* **2009**, *131*, 4619.
[3] S.-I. Tanaka, J. Miyazaki, D. K. Tiwari, T. Jin, Y. Inouye, *Angew. Chem.* **2011**, *123*, 451; *Angew. Chem. Int. Ed.* **2011**, *50*, 431.
[4] M. Mahmoudi, V. Serpooshan, S. Laurent, *Nanoscale* **2011**, *3*, 3007.
[5] A. A. Cordones, M. Scheele, A. P. Alivisatos, S. R. Leone, *J. Am. Chem. Soc.* **2012**, *134*, 18366.
[6] F. Wang, X. G. Liu, *Chem. Soc. Rev.* **2009**, *38*, 976.
[7] H. C. Guo, S. Q. Sun, *Nanoscale* **2012**, *4*, 6692.
[8] S. N. Baker, G. A. Baker, *Angew. Chem.* **2010**, *122*, 6876; *Angew. Chem. Int. Ed.* **2010**, *49*, 6726.
[9] L. Zhou, Y. Lin, Z. Huang, J. S. Ren, X. Qu, *Chem. Commun.* **2012**, *48*, 1147.
[10] T. G. Schaaff, R. L. Whetten, *J. Phys. Chem. B* **2000**, *104*, 2630.
[11] R. Guo, Y. Song, G. Wang, R. W. Murray, *J. Am. Chem. Soc.* **2005**, *127*, 2752.
[12] Y. Shichibu, Y. Negishi, T. Tsukuda, T. Teranishi, *J. Am. Chem. Soc.* **2005**, *127*, 13464.
[13] Y. Shichibu, Y. Negishi, T. Watanabe, N. K. Chaki, H. Kawaguchi, T. Tsukuda, *J. Phys. Chem. C* **2007**, *111*, 7845.
[14] P. D. Jadzinsky, G. Calero, C. J. Ackerson, D. A. Bushnell, R. D. Kornberg, *Science* **2007**, *318*, 430.

[15] M. Zhu, E. Lanni, N. Garg, M. E. Bier, R. Jin, *J. Am. Chem. Soc.* **2008**, *130*, 1138.
[16] H. Qian, W. T. Eckenhoff, M. E. Bier, T. Pintauer, R. Jin, *Inorg. Chem.* **2011**, *50*, 10735.
[17] Z. Wu, R. Jin, *Nano Lett.* **2010**, *10*, 2568.
[18] M. S. Devadas, J. Kim, E. Sinn, D. Lee, T. Goodson III, G. Ramakrishna, *J. Phys. Chem. C* **2010**, *114*, 22417.
[19] Y. Bao, H. C. Yeh, C. Zhong, S. A. Ivanov, J. K. Sharma, M. L. Neidig, D. M. Vu, A. P. Shreve, R. B. Dyer, J. H. Werner, J. S. Martinez, *J. Phys. Chem. C* **2010**, *114*, 15879.
[20] H. Qian, W. T. Eckenhoff, Y. Zhu, T. Pintauer, R. Jin, *J. Am. Chem. Soc.* **2010**, *132*, 8280.
[21] X. Meng, Q. Xu, S. Wang, M. Zhu, *Nanoscale* **2012**, *4*, 4161.
[22] H. Qian, Y. Zhu, R. Jin, *Proc. Natl. Acad. Sci. USA* **2012**, *109*, 696.
[23] Z. Tang, T. Ahuja, S. Wang, G. Wang, *Nanoscale* **2012**, *4*, 4119.
[24] H. Wu, H. Zhu, J. Zhuang, S. Yang, C. Liu, Y. C. Cao, *Angew. Chem.* **2008**, *120*, 3790; *Angew. Chem. Int. Ed.* **2008**, *47*, 3730.
[25] C. J. Lin, C. H. Lee, J. T. Hsieh, H.-H. Wang, J. K. Li, J. L. Shen, W. H. Chang, H. I. Yeh, W. H. Chang, *J. Med. Biol. Eng.* **2009**, *29*, 276.
[26] C. J. Lin, T. Y. Yang, C. H. Lee, S. H. Huang, R. A. Sperling, M. Zanella, J. K. Li, J. L. Shen, H. H. Wang, H. I. Yeh, W. J. Parak, W. H. Chang, *ACS Nano* **2009**, *3*, 395.
[27] L. Polavarapu, M. Manna, Q. H. Xu, *Nanoscale* **2011**, *3*, 429.
[28] F. Wen, Y. Dong, L. Feng, S. Wang, S. Zhang, X. Zhang, *Anal. Chem.* **2011**, *83*, 1193.
[29] X. L. Guével, N. Daum, M. Schneider, *Nanotechnology* **2011**, *22*, 275103.
[30] L. Shang, R. M. Dörlich, V. Trouillet, M. Bruns, G. U. Nienhaus, *Nano Res.* **2012**, *5*, 531.
[31] L. Shang, N. Azadfar, F. Stockmar, W. Send, V. Trouillet, M. Bruns, D. Gerthsen, G. U. Nienhaus, *Small* **2011**, *7*, 2614.
[32] J. Zheng, J. T. Petty, R. M. Dickson, *J. Am. Chem. Soc.* **2003**, *125*, 7780.
[33] L. Shang, S. J. Dong, *Chem. Commun.* **2008**, 1088.
[34] R. Zhou, M. Shi, X. Chen, M. Wang, H. Chen, *Chem. Eur. J.* **2009**, *15*, 4944.
[35] W.-Y. Chen, G.-Y. Lan, H.-T. Chang, *Anal. Chem.* **2011**, *83*, 9450.
[36] M. A. H. Muhammed, S. Ramesh, S. S. Sinha, S. K. Pal, T. Pradeep, *Nano Res.* **2008**, *1*, 333.
[37] J. Xie, Y. Zheng, J. Y. Ying, *J. Am. Chem. Soc.* **2009**, *131*, 888.
[38] H. Kawasaki, K. Hamaguchi, I. Osaka, R. Arakawa, *Adv. Funct. Mater.* **2011**, *21*, 3508.
[39] X. L. Guével, C. Spies, N. Daum, G. Jung, M. Schneider, *Nano Res.* **2012**, *5*, 379.
[40] X. Yuan, Z. Luo, Q. Zhang, X. Zhang, Y. Zheng, J. Y. Lee, J. Xie, *ACS Nano* **2011**, *5*, 8800.
[41] T.-H. Cheng, W. L. Tseng, *Small* **2012**, *8*, 1912.
[42] X. Wen, P. Yu, Y. R. Toh, J. Tang, *J. Phys. Chem. C* **2012**, *116*, 11830.
[43] P. L. Xavier, K. Chaudhari, A. Baksi, T. Pradeep, *Nano Rev.* **2012**, *3*, 14767.
[44] P.-C. Cheng, C.-K. Chiang, H.-T. Chang, *J. Nanopart. Res.* **2013**, *15*, 1336.
[45] J. Zheng, P. R. Nicovich, R. M. Dickon, *Annu. Rev. Phys. Chem.* **2007**, *58*, 409.
[46] J. Zheng, C. Zhou, M. Yu, J. Liu, *Nanoscale* **2012**, *4*, 4073.
[47] H. Qian, M. Zhu, Z. Wu, R. Jin, *Acc. Chem. Res.* **2012**, *45*, 1470.
[48] C. A. Fields-Zinna, M. C. Crowe, A. Dass, J. E. F. Weaver, R. W. Murray, *Langmuir* **2009**, *25*, 7704.
[49] Y. Negishi, K. Igarashi, K. Munakata, W. Ohgake, K. Nobusada, *Chem. Commun.* **2012**, *48*, 660.
[50] Y. Negishi, T. Iwai, M. Ide, *Chem. Commun.* **2010**, *46*, 4713.
[51] C. Kumara, A. Dass, *Nanoscale* **2012**, *4*, 4084.
[52] C. Kumara, A. Dass, *Nanoscale* **2011**, *3*, 3064.
[53] H. Qian, D. Jiang, G. Li, C. Gayathri, A. Das, R. R. Gil, R. Jin, *J. Am. Chem. Soc.* **2012**, *134*, 16159.
[54] S. Y. Park, D. Lee, *Langmuir* **2012**, *28*, 7049.
[55] K. Nobusada, T. Iwasa, *J. Phys. Chem. C* **2007**, *111*, 14279.
[56] M. Y. Sfeir, H. Qian, K. Nobusada, R. Jin, *J. Phys. Chem. C* **2011**, *115*, 6200.
[57] H. Qian, M. Zhu, C. Gayathri, R. R. Gil, R. Jin, *ACS Nano* **2011**, *5*, 8935.

